

www.acsanm.org Article

Substrate-Induced Modulation of Quantum Emitter Properties in 2D Hexagonal Boron Nitride: Implications for Defect-Based Single Photon Sources in 2D Layers

Sai Krishna Narayanan and Pratibha Dev*



Cite This: ACS Appl. Nano Mater. 2023, 6, 3446–3452

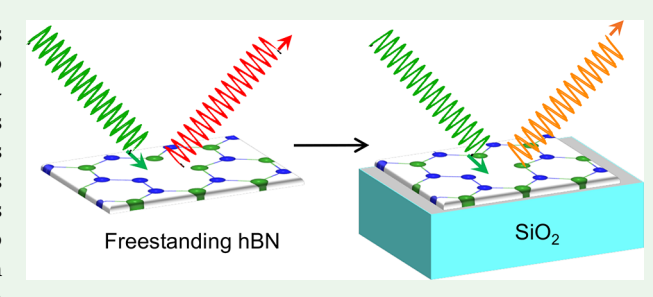


ACCESS

III Metrics & More

Article Recommendations

ABSTRACT: Quantum emitters (QEs) based on deep-level defects in hexagonal boron nitride (hBN) layers are promising alternatives to other qubit-candidates in three-dimensional wide bandgap semiconductors. The two-dimensional (2D) form factor of hBN allows the possibility of near-deterministic placement of quantum emitters and an ease of property-tuning via different means, such as application of strain. However, the 2D nature of hBN also results in a unique set of challenges, including a sensitivity of the QEs to their environment that can influence their different properties, such as their emission frequencies and brightness. In particular, although



observed experimentally, theoretical works thus far have ignored substrate-induced modulation of hBN's QE properties. As a result, to date, the magnitude of substrate effects and the underlying mechanism(s) involved in the modulation of QE properties remain unknown. In our density functional theory-based work, we use silicon dioxide as a prototype substrate to demonstrate that the substrate effects can indeed have a significant impact on ground- and excited-state properties of defects responsible for quantum emission. Our analysis shows large structural distortions at the defect sites due to substrate interactions, resulting in significant changes in quantum emission frequencies. These calculations reveal that accounting for substrate effects is critical to the successful use of hBN in quantum sensing and quantum computing.

KEYWORDS: quantum emitters, 2D hexagonal boron nitride, point defects, substrate effects, optical property modulation, density functional theory

■ INTRODUCTION

The atom/molecule-like optical properties of the deep level defects in hexagonal boron nitride (hBN) layers make them promising solid-state quantum emitters (QEs) for use in quantum sensing and quantum computing. What gives QEs in hBN such a tremendous potential are the different advantages offered by the two-dimensional (2D) layered structure of the host material as compared to three-dimensional semiconductor hosts, such as different SiC polytypes and diamond. These advantages include a possibility of deterministic placement of defects in a 2D host and a greater ability to tune properties of the defects in 2D layers. The latter can be achieved via a number of means, such as chemical alterations (doping) of the layers, application of strain, and/or simple heterostructuring.

Notwithstanding the aforementioned potential advantages of using hBN as a host to QEs, there are several challenges to using its defects in quantum applications. The biggest hurdle is that, to date, the chemical nature of the fluorescent defects in hBN has remained unknown. In large part, this challenge arises because a significant number of intrinsic and extrinsic defects in hBN are deep level defects, resulting in a large and complex

chemical phase space for defect-based QEs in hBN. Although some advances have been made in narrowing down candidate defects, ^{1,5,29–33} their exact chemical nature is still debated. The difficulties in identifying the precise defects responsible for quantum emission are compounded by large variations in the defect properties, even if the defects are assumed to be the same species. ^{5,6} The observed variations in different properties, such as the brightness and emission frequencies, are often attributed to differing local strains at the defect sites. A recent theoretical work³⁴ explained how strain can modify different properties of hBN defects. Within an hBN sample, there can be a number of sources of strain, including the presence of other point/extended defects in the vicinity and/or grain boundaries. Another source of strain that has not received much attention

Received: December 5, 2022 Accepted: February 7, 2023 Published: February 17, 2023





ACS Applied Nano Materials

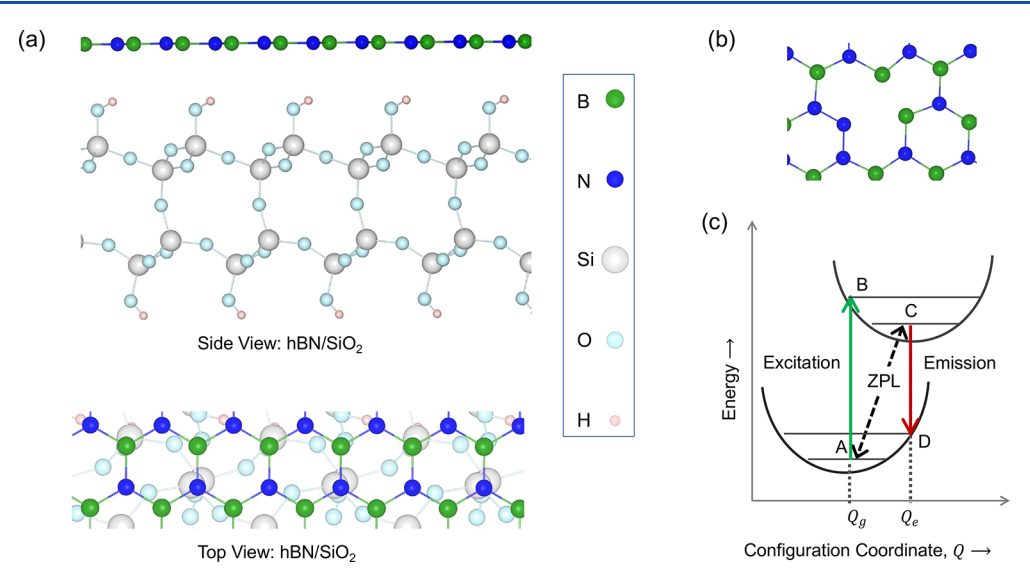


Figure 1. Elucidating substrate-effects on defect-based quantum emitters (QEs) in hBN. (a) The side view and top view, showing equilibrium structure of the pristine hBN/SiO₂ composite. (b) The antisite defect complex, V_NN_B , investigated in this proof-of-principle study. (c) Energy vs configuration coordinate (Q) diagram illustrating Franck—Condon principle applied to light absorption and emission by the defect center, which is used to obtain the zero phonon line (ZPL) of the defect within constrained-occupation DFT (CDFT). Within CDFT, total energies corresponding to different ionic and electronic configurations for points A, B, C, and D are calculated, with the C \leftrightarrow A transition corresponding to the ZPL.

is the substrate itself. The importance of substrate effects can be seen in the experimental report by Exarhos et al.⁶ The main goal of Exarhos et al. was to eliminate substrate effects by characterizing single-photon sources in hBN suspended on etched holes in a patterned Si/SiO2 substrate. Nevertheless, their extensive study also reported a non-negligible perturbation of QE properties in supported regions of hBN as compared to those QEs in suspended regions. As the observed substrate-dependence of the optical properties was outside the scope of their study, it was not pursued beyond providing several conjectures regarding its origin. In fact, thus far, the nature of hBN-substrate interactions has remained unexplored in theoretical and experimental studies. As a result, it is not known how and to what extent these interactions modify the properties of the hBN layer and its defects. For example, it is not clear if the substrate effects can result in structural distortions and hence strain at a defect site, quenching of the defect spin, and/or changes in the frequency of its quantum emission, even if the defect spin state is stable. This lack of understanding of substrate effects represents a serious knowledge gap as revealed by recent theoretical works on other layered materials, 35-38 which show that the interactions between 2D layers and their mixed/heterodimensional or homodimensional substrates can modify different properties of the 2D-layers substantially and in unpredictable ways. In this theoretical work, we explore substrate-hBN interactions and demonstrate how these interactions affect the ground- and excited-state properties of quantum emitters within hBN.

■ RESULTS AND DISCUSSION

Spin-resolved density-functional theory (DFT) calculations were carried out using the Quantum-ESPRESSO package. To study substrate effects, we placed an hBN monolayer on a fully passivated (111)-oriented β -cristobalite slab, 40,41 which is a polymorph of SiO₂ (see Methods for details). SiO₂ was chosen as the substrate due to its experimental relevance. Figure 1(a) shows the top and side views of the hBN/SiO₂ composite. Within this mixed-dimensional heterostructure, the

pristine hBN monolayer remains planar, as can be seen in Figure 1(a). It is physisorbed onto the fully passivated SiO_2 surface, with a binding energy per unit area, E_b /area, of -10.8 meV/Ų. The binding energy is defined as $E_b = E_{hBN/SiO_2} - \{E_{hBN} + E_{SiO_2}\}$, where the hBN and SiO_2 geometries are those found in the composite. Using Löwdin charge analysis, we find that there is a net charge transfer of 0.21 electrons from hBN to SiO_2 . This is owing to the small difference in the work functions of the two components, with the work functions being 5.82 and 6.59 eV for pristine hBN and the fully passivated SiO_2 , respectively. Here the work function is obtained from the difference between the electrostatic potential in the vacuum region (far from the surface) and the highest occupied state, i.e. the valence band maximum, assuming that the Fermi level is at the band edge.

As mentioned in Introduction, there are many candidate intrinsic and extrinsic, spin-active point defects in hBN. One needs to consider the nature of orbitals from which the defect states are derived in order to understand why most of the hBN defects are spin-active, deep-level defects. Most of the defect states are (sp²-hybridized) dangling bonds derived from the highly localized 2s- and 2p-states of boron and/or nitrogen atoms surrounding the defects. The localized nature of the orbitals involved in the defect states, 42,43 along with additional quantum confinement effects due to the reduced dimension of the host matrix, 20,34,44 result in a large exchange interaction between the electrons in the partially filled dangling bonds. This in turn results in spin-polarized structures with an excess of electrons in one spin channel (majority spin) over the other (minority-spin channel). Many of these spin-active deep defects can potentially be QEs. In this proof-of-principle study, we considered a neutral antisite complex $(V_N N_B)$. This intrinsic defect consists of a nitrogen vacancy next to a nitrogen substitutional [Figure 1(b)]. This is one of the leading candidate defects and has been postulated to be responsible for hBN's quantum emission in several works. 1,5,45,46 To study the effects of the substrate on the excited-state properties of the V_NN_B complex, we calculated

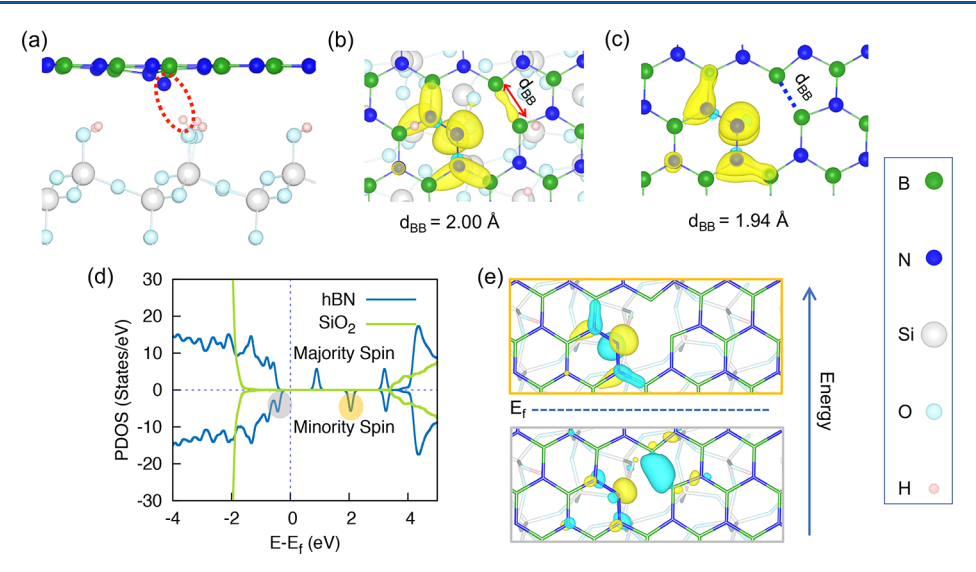


Figure 2. (a) Ground-state equilibrium geometry of defective hBN placed on substrate, showing the introduction of sp³ character in hBN and straining of its matrix. The weak bond between N_B of V_NN_B defect and the H atom of the passivated SiO_2 is highlighted by circling those atoms in red. (b) Spin density plot (difference in charge densities within the two spin channels) for the defect in hBN/ SiO_2 heterostructure, showing the localized nature of the defect states. The boron—boron distance, d_{BB} , is 2.00 Å for this structure. (c) Spin density plot for the V_NN_B complex in the freestanding hBN. (d) Density of states (DOS) projected onto defective hBN and SiO_2 within the hBN/ SiO_2 heterostructure. The contribution of the defective hBN to the total DOS shows the spin-splitting between the two spin channels, along with the localized nature of defect states as can be seen by the sharp peaks that are introduced in the bandgap of hBN. The sharp peaks highlighted in gray and orange colors are the filled and empty minority-spin defect states, respectively, which are involved in the lowest energy optical excitation. (e) Charge density plots showing the filled and empty minority-spin states involved in the excitation. For the sake of clarity, a stick model is used to represent the atomic structure in both volumetric plots. Yellow (blue) colors correspond to positive (negative) isovalues.

the zero phonon line (ZPL) for the defect using constrained-occupation DFT (CDFT), followed by mapping of the results onto the Franck-Condon picture, which is illustrated in Figure 1(c) (see Methods for details).

Ground-State Properties of V_NN_B. Before investigating the effects of the substrate on the V_NN_B complex in hBN, we calculated the properties of the defect within a freestanding hBN monolayer. In a freestanding monolayer, V_NN_B possesses a C_{2V} point-group symmetry, as can be seen in Figure 1(b). The two boron atoms, which are adjacent to the nitrogen vacancy of the V_NN_B complex, form a weak covalent bond with a bond length, $d_{\rm BB}$, of 1.94 Å in the ground-state equilibrium geometry (GEG), in agreement with the reported bond length in a previous work. The V_NN_B complex is a spin-1/2 defect with a large spin polarization energy of 227.54 meV, which implies that the spin of the defect will survive beyond room temperature ($k_{\rm B}T\approx 25$ meV). The spin polarization energy is obtained from the difference between total energies of spin-unpolarized and spin-polarized calculations.

To elucidate how substrates themselves can modify groundand excited-state properties of defects in hBN, we created a neutral $V_{\rm N}N_{\rm B}$ complex in the hBN monolayer on the SiO₂ substrate. Due to the substrate, the symmetry of the defect reduces from the C_{2V} point-group symmetry for freestanding hBN to a much lower C_1 -symmetry. The binding energy per unit area for the defective hBN/SiO₂ is found to be -12.80meV/Å². This is a relatively small increase in $E_{\rm b}$ /area compared to that for pristine hBN/SiO₂. The increase in the binding energy mostly comes from a very weak bond that is formed between the N_B of the defect complex and one of the hydrogens on the SiO₂ surface. The atoms involved in this weak bond are circled in red in Figure 2(a). The N_B-H distance within the heterostructure is found to be 1.72 Å, as compared to the N-H distance of 2.55 Å in the case of pristine hBN/SiO₂ (also, compare to the N–H distance of 1.01 Å in NH₃). The formation of the weak bond between an H atom from the passivated SiO₂ film and N_B of the defect complex is facilitated by the buckling of the hBN sheet, as seen in Figure 2(a). This structural distortion introduces an sp³ character to the hBN layer. Concomitant to these out-of-plane distortions, the weak covalent bond between boron atoms surrounding the defect weakens, with $d_{\rm BB}$ increasing to 2.00 Å [see Figure 2(b)] from a value of 1.94 Å for the freestanding hBN, shown in Figure 2(c). In addition, from the Löwdin charge analysis, we find that there is an additional net charge of 0.09 electrons on the defective hBN layer within the composite as compared to the freestanding defective hBN.

Although the structural distortions around the V_NN_B defect in hBN/SiO₂ are large, we find that there is no quenching of its spin, and V_NN_B is still a spin-1/2 defect. The spatial distribution of this spin-1/2 is visualized via the spin density plot in Figure 2(b), which gives the difference in charge densities within majority and minority-spin channels $\Delta \rho =$ $ho^{
m Maj~Spin}ho^{
m Min~Spin}$]. Figure 2(b) shows that even in the mixeddimensional heterostructure, most of the spin-1/2 of the defect comes from the atoms surrounding the defect, just as is the case for the V_NN_B complex in the freestanding hBN [see Figure 2(c) for comparison]. We also find the spin polarization energy to be 560.93 eV for V_NN_B in hBN/SiO₂, which is much larger than that for the defective freestanding hBN (see Table 1). The larger value of spin polarization energy for the defect in hBN/SiO₂ can be attributed to the enhanced spatial localization of the defect states in the heterostructure. The latter is caused by the greater distances between the atoms surrounding the defect within hBN on SiO2, as compared to those in freestanding hBN. These atoms show local out-of-plane distortions in the presence of a substrate. The extent of spinsplitting among the defect states and their localized nature can

Table 1. Properties of the Neutral V_NN_B Defect in the Freestanding hBN Monolayer and within the hBN/SiO₂ Composite^a

optically active spin channel	spin	$E_{\rm pol}~({ m meV})$	system
minority spin	1/2	227.54	hBN
minority spin	1/2	560.93	hBN/SiO2

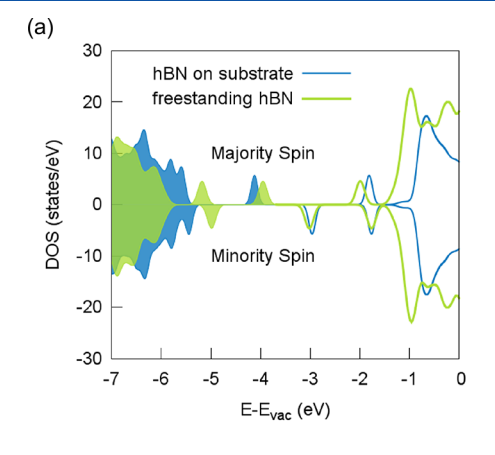
"Here, the spin polarization energy, $E_{\rm pol}$ is obtained from the difference between total energies of spin-unpolarized $(E_{\rm spin\ unpol})$ and spin-polarized $(E_{\rm spin\ pol})$ calculations: $E_{\rm pol}=E_{\rm spin\ unpol}-E_{\rm spin\ pol}$. The spin channel involved in the lowest energy excitation is also indicated.

be seen in the density of states (DOS) plot in Figure 2(d), which is a plot of DOS projected onto the two components, SiO_2 and hBN, in the heterostructure. Table 1 also gives the spin channel involved in the lowest-energy optical excitations, which remains the minority spin channel for the defect in the heterostructure, just like in the freestanding hBN. These states are highlighted in the DOS plot (in gray and orange) of Figure 2(d) and are shown as charge density plots in Figure 2(e), displaying their localized nature. In the remainder of the work, we concentrate on the spin-preserving optical excitation between these two states to elucidate the effect of the substrate on their quantum emission.

Excited-State Properties of V_NN_B. To study the effect of the substrate on the excited-state properties of the V_NN_B defect complex, we used CDFT to calculate the ZPL of the defect with and without the substrate. We find that the ZPL of the antisite defect complex in hBN/SiO₂ is 0.22 eV higher than the ZPL of an antisite complex within freestanding hBN. This change in ZPL can be directly attributed to the substrate interaction, which results in the changes in the local structure around the defect [see Figure 2(a)]. These structural distortions induce local strain at the defect site, which is expected to affect the placement of the defect levels within hBN's bandgap as compared to their placement and their separation for freestanding hBN. Figure 3(a) shows that this is indeed the case by comparing the DOS for defective hBN in the hBN/SiO₂ heterostructure with the DOS for a freestanding hBN monolayer with a $V_{\rm N}N_{\rm B}$ defect. To facilitate the comparison, the DOS plots are made with respective vacuum

levels as the reference energies for the two structures. In addition, the filled (empty) curves represent the filled (empty) states. Concentrating on the defect states from the minority spin channel that are involved in the lowest energy photoexcitation, one can see that the heterostructure formation more strongly affects the position of the filled defect state, which is now at the edge of the valence band as compared to the empty state. The empty defect state of the heterostructure almost perfectly overlaps with the corresponding state in freestanding hBN. The disparate responses of the filled and empty minority spin states to the heterostructure formation are a consequence of their bonding nature. The filled state [Figure 2(e), bottom plot shows a predominant antibonding character between N_B and the two weakly bonded borons. This state is, therefore, stabilized as a result of increased distances between the atoms surrounding the defect, owing to its interactions with the substrate. On the other hand, for the empty minority state [Figure 2(e), top charge density plot], which is involved in the spin preserving excitation, the charge density is mostly localized on N_B. As a result, it is minimally affected by the substrate-induced distortion/local strain around the defect. The resulting difference of 0.22 eV in the quantum emission frequencies of the antisite complex within freestanding hBN and hBN/SiO₂ might in part explain the experimentally observed spectral spread of ≈0.2 eV in the photoluminescence spectra of defects reported by Grosso et al.

It is also interesting to note that the Stokes shift for defective hBN on SiO_2 is 0.93 eV, which is much larger than the Stokes shift calculated for the freestanding unstrained hBN (0.59 eV). The theoretical values of Stokes shifts were obtained from the difference in the vertical excitation and the ZPL, i.e. by calculating the total energy differences between points B and C in the Franck–Condon picture of Figure 1(c). This large increase in the Stokes shift is indicative of large changes in the local atomic structure around the defect following the vertical excitation. This can indeed be seen in the excited-state equilibrium geometry (EEG) of the defect shown in Figure 3(b). It shows a complete breaking of the weak N_B –H bond (with an EEG distance of 2.12 Å between N_B and H), and as a result, a near-perfect restoration of the local sp² structure of hBN in the excited state.



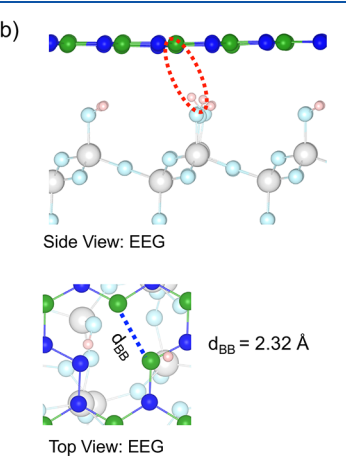


Figure 3. Excited state properties: (a) A comparison of the DOS for defective hBN in the hBN/SiO₂ heterostructure with the DOS for freestanding hBN with a V_NN_B defect. The respective vacuum levels (E_{vac}) of the two structures are used as the reference energies. Filled (empty) curves represent the filled (empty) states. (b) Excited-state equilibrium geometry (EEG) showing the return of hBN to a planar structure in the excited state and a large concomitant rearrangement of atoms around the defect. The complete breaking of weak bond between N_B and the H atom in the excited state is highlighted by circling those atoms in red.

CONCLUSION

In any application of the bright and robust QEs of hBN in quantum computing and quantum sensing, it is expected that the host hBN crystal itself will be placed on either a 2D or a 3D substrate. However, thus far, hBN-substrate interactions have not been studied theoretically, even though noted in an experiment.⁶ In our work, we have highlighted this serious knowledge gap by isolating effects of substrates on QE properties, while eliminating other sources of perturbation within hBN layers (such as other defects, layer thickness, and grain boundaries). Our analysis demonstrates that the substrate interactions can have non-negligible effects on different properties of defects in hBN. In particular, we showed that a defective hBN layer interacts more strongly with the substrate, resulting in an out-of-plane distortion and, as a result, to strain in the layer. The response of the defect states to substrateinduced local strains around defect sites changes the quantum emission frequency of the defects in the hBN layer on a substrate. Hence, although in experiments there are undoubtedly other sources of property perturbations, the substrates themselves are, at least in part, responsible for the wide ranges of properties displayed by hBN QEs. Our work shows that to properly understand the properties of hBN QEs as reported by experiments and to ultimately use this layered material in quantum technologies, it is imperative to take substrate effects into account.

METHODS

Spin-polarized DFT calculations were performed using the QUANTUM ESPRESSO package.³⁹ The generalized gradient approximation (GGA)⁴⁷ of Perdew-Burke-Ernzerhof (PBE)⁴⁸ was used to account for the exchange-correlation effects. All results for the pristine and defective hBN were obtained using a $6 \times 6 \times 1$ (72atoms) supercell of hBN. To study substrate effects, we placed this 72-atom hBN monolayer on a SiO₂ substrate, which was chosen due to its experimental relevance.⁶ For SiO_2 , we used a (111)-oriented β cristobalite seven-layer slab, employing the structure described by Wehling et al. 40 and Bermudez et al. 41 Bulk β -cristobalite has $Fd\overline{3}m$ space group symmetry (#227). The lattice constant of bulk ${\rm SiO_2}$ is $a_{{\rm SiO_2}}=7.13~{\rm \AA}^{.49}$ As a result, the lattice constant of the surface unit cell for the (111)-oriented β -cristobalite is $a_{SiO_2}/\sqrt{2} = 5.04$ Å, which is only 0.40% larger than twice that of the hBN unit cell ($2a_{\rm hBN} = 5.02$ Å). Because the lattice mismatch is small, we constructed a commensurate hBN/SiO $_2$ heterostructure unit cell by placing a 2 \times 2×1 hBN supercell on the unit cell for the β -cristobalite (111) surface, fixing the lattice constant to be $2a_{hBN}$ for the heterostructure unit cell. To study properties of defects within hBN/SiO2, we constructed a 3 \times 3 \times 1 supercell from the aforementioned commensurate hBN/SiO₂ heterostructure unit cell [Figure 1(a)]. Because the lattice constant of the resulting heterostructure supercell is the same as that of the freestanding (72-atom) hBN supercell, it allowed a direct comparison of the defect properties in freestanding hBN and hBN on the substrate. It is also important to note that the dangling bonds of freshly cleaved SiO₂ are very reactive; an exposed SiO₂ surface is expected to get fully passivated through water dissociation. Hence, the SiO2 slab used in this work was fully hydroxylated on both sides by the addition of hydrogen (H) on one side and hydroxyl groups (OH) on the other side, passivating the dangling bonds. ⁴¹ To correctly describe the interactions between hBN and fully passivated SiO₂, we employed Grimme's DFT-D2 van der Waals (vdW) corrections.⁵⁰ The Monkhorst–Pack scheme⁵¹ was used to create a Γ -centered, $4 \times 4 \times 1$ k-point grid to sample the Brillouin zone. The composite hBN/SiO₂ structures were relaxed while keeping the lower layers of SiO2 fixed. A vacuum layer of 20 Å was added in the direction normal to the surfaces of both freestanding hBN and

 ${\rm hBN/SiO_2}$ heterostructure to eliminate the spurious interactions between the periodic images of the respective structures.

Excited-state properties of the V_NN_B antisite complex in freestanding hBN and hBN on the substrate were calculated using CDFT, followed by the mapping of the results onto the Franck-Condon picture, 22 which is illustrated in Figure 1(c). Within the CDFT method, the photoluminescence process is mimicked by constraining the occupation of the defect states via the promotion of an electron from the highest occupied defect state in the optically active spin channel to the previously unoccupied defect state of the same spin. The structure is then allowed to relax with this new electronic configuration. Finally, another self-consistent calculation is performed with these excited-state ionic positions, but allowing the electron to return to its ground-state electronic configuration. These different electronic and ionic configurations provide the total energies corresponding to points A, B, C, and D in the Franck-Condon picture [Figure 1(c)], where it is assumed that the electronic transition upon the absorption or emission of photons happens much faster than the rearrangement of the ions. Hence, the absorption corresponds to the vertical transition from A → B in the Franck-Condon picture, the transition $C \leftrightarrow A$ corresponds to the ZPL, and the emission of a photon corresponds to the vertical transition from C

AUTHOR INFORMATION

Corresponding Author

Pratibha Dev — Department of Physics and Astronomy, Howard University, Washington, D.C. 20059, United States; orcid.org/0000-0002-6884-6737; Email: pratibha.dev@howard.edu

Author

Sai Krishna Narayanan – Department of Physics and Astronomy, Howard University, Washington, D.C. 20059, United States

Complete contact information is available at: https://pubs.acs.org/10.1021/acsanm.2c05233

Notes

The authors declare no competing financial interest.

ACKNOWLEDGMENTS

This work is supported by the National Science Foundation (NSF grants no. DMR-1752840, no. OMA-2231278, and no. EEC-1941583). This work used the Expanse and Bridges2 clusters at SDSC and PSC, respectively, through allocation PHY180014 from the Advanced Cyberinfrastructure Coordination Ecosystem: Services & Support (ACCESS) program, which is supported by National Science Foundation grants no. 2138259, no. 2138286, no. 2138307, no. 2137603, and no. 2138296.

REFERENCES

- (1) Tran, T. T.; Bray, K.; Ford, M. J.; Toth, M.; Aharonovich, I. Quantum emission from hexagonal boron nitride monolayers. *Nat. Nanotechnol.* **2016**, *11*, 37.
- (2) Tran, T. T.; Elbadawi, C.; Totonjian, D.; Lobo, C. J.; Grosso, G.; Moon, H.; Englund, D. R.; Ford, M. J.; Aharonovich, I.; Toth, M. Robust multicolor single photon emission from point defects in hexagonal boron nitride. *ACS Nano* **2016**, *10*, 7331–7338.
- (3) Choi, S.; Tran, T. T.; Elbadawi, C.; Lobo, C.; Wang, X.; Juodkazis, S.; Seniutinas, G.; Toth, M.; Aharonovich, I. Engineering and localization of quantum emitters in large hexagonal boron nitride layers. ACS Appl. Mater. Interfaces 2016, 8, 29642—29648.
- (4) Martínez, L. J.; Pelini, T.; Waselowski, V.; Maze, J. R.; Gil, B.; Cassabois, G.; Jacques, V. Efficient single photon emission from a

- high-purity hexagonal boron nitride crystal. Phys. Rev. B 2016, 94, 121405.
- (5) Grosso, G.; Moon, H.; Lienhard, B.; Ali, S.; Efetov, D. K.; Furchi, M. M.; Jarillo-Herrero, P.; Ford, M. J.; Aharonovich, I.; Englund, D. Tunable and High Purity Room-Temperature Single Photon Emission from Atomic Defects in Hexagonal Boron Nitride. *Nat. Commun.* 2017, 8, 705.
- (6) Exarhos, A. L.; Hopper, D. A.; Grote, R. R.; Alkauskas, A.; Bassett, L. C. Optical Signatures of Quantum Emitters in Suspended Hexagonal Boron Nitride. *ACS Nano* **2017**, *11*, 3328.
- (7) Tran, T. T.; Kianinia, M.; Nguyen, M.; Kim, S.; Xu, Z.-Q.; Kubanek, A.; Toth, M.; Aharonovich, I. Resonant Excitation of Quantum Emitters in Hexagonal Boron Nitride. *ACS Photonics* **2018**, *5*, 295–300.
- (8) Proscia, N. V.; Shotan, Z.; Jayakumar, H.; Reddy, P.; Cohen, C.; Dollar, M.; Alkauskas, A.; Doherty, M.; Meriles, C. A.; Menon, V. M. Near-deterministic activation of room-temperature quantum emitters in hexagonal boron nitride. *Optica* **2018**, *5*, 1128–1134.
- (9) Abdi, M.; Chou, J.-P.; Gali, A.; Plenio, M. B. Color Centers in Hexagonal Boron Nitride Monolayers: A Group Theory and Ab Initio Analysis. *ACS Photonics* **2018**, *5*, 1967–1976.
- (10) Ziegler, J.; Klaiss, R.; Blaikie, A.; Miller, D.; Horowitz, V. R.; Alemán, B. J. Deterministic Quantum Emitter Formation in Hexagonal Boron Nitride via Controlled Edge Creation. *Nano Lett.* **2019**, *19*, 2121–2127.
- (11) Gale, A.; Li, C.; Chen, Y.; Watanabe, K.; Taniguchi, T.; Aharonovich, I.; Toth, M. Site-Specific Fabrication of Blue Quantum Emitters in Hexagonal Boron Nitride. *ACS Photonics* **2022**, *9*, 2170–2177.
- (12) Tan, Q.; Lai, J.-M.; Liu, X.-L.; Guo, D.; Xue, Y.; Dou, X.; Sun, B.-Q.; Deng, H.-X.; Tan, P.-H.; Aharonovich, I.; Gao, W.; Zhang, J. Donor—Acceptor Pair Quantum Emitters in Hexagonal Boron Nitride. *Nano Lett.* **2022**, *22*, 1331–1337.
- (13) Shaik, A. B. D.; Palla, P. Optical quantum technologies with hexagonal boron nitride single photon sources. *Sci. Rep.* **2021**, *11*, 12285
- (14) Weber, J. R.; Koehl, W. F.; Varley, J. B.; Janotti, A.; Buckley, B. B.; Van de Walle, C. G.; Awschalom, D. D. Defects in SiC for quantum computing. *J. Appl. Phys.* **2011**, *109*, 102417.
- (15) Carter, S. G.; Soykal, O. O.; Dev, P.; Economou, S. E.; Glaser, E. R. Spin coherence and echo modulation of the silicon vacancy in 4*H* SiC at room temperature. *Phys. Rev. B* **2015**, 92, 161202.
- (16) Soykal, O.; Dev, P.; Economou, S. E. Silicon vacancy center in 4 H-SiC: Electronic structure and spin-photon interfaces. *Phys. Rev. B* **2016**, 93, 081207.
- (17) Economou, S. E.; Dev, P. Spin-photon entanglement interfaces in silicon carbide defect centers. *Nanotechnology* **2016**, 27, 504001.
- (18) Lukin, D. M.; Dory, C.; Guidry, M. A.; Yang, K. Y.; Mishra, S. D.; Trivedi, R.; Radulaski, M.; Sun, S.; Vercruysse, D.; Ahn, G. H.; Vučković, J. 4H-silicon-carbide-on-insulator for integrated quantum and nonlinear photonics. *Nat. Photonics* **2020**, *14*, 330–334.
- (19) Lukin, D. M.; White, A. D.; Trivedi, R.; Guidry, M. A.; Morioka, N.; Babin, C.; Soykal, Ö. O.; Ul-Hassan, J.; Son, N. T.; Ohshima, T.; Vasireddy, P. K.; Nasr, M. H.; Sun, S.; MacLean, J. W.; Dory, C.; Nanni, E. A.; Wrachtrup, J.; Kaiser, F.; Vuckovic, J. Spectrally reconfigurable quantum emitters enabled by optimized fast modulation. *npj Quantum Information* **2020**, *6*, 80.
- (20) Joshi, T.; Dev, P. Site-Dependent Properties of Quantum Emitters in Nanostructured Silicon Carbide. *PRX Quantum* **2022**, *3*, 020325.
- (21) Balasubramanian, G.; Chan, I. Y.; Kolesov, R.; Al-Hmoud, M.; Tisler, J.; Shin, C.; Kim, C.; Wojcik, A.; Hemmer, P. R.; Krueger, A.; Hanke, T.; Leitenstorfer, A.; Bratschitsch, R.; Jelezko, F.; Wrachtrup, J. Nanoscale imaging magnetometry with diamond spins under ambient conditions. *Nature* **2008**, *455*, 648–651.
- (22) Gali, A.; Janzén, E.; Deák, P.; Kresse, G.; Kaxiras, E. Theory of Spin-Conserving Excitation of the $N-V^-$ Center in Diamond. *Phys. Rev. Lett.* **2009**, 103, 186404.

- (23) Stanwix, P. L.; Pham, L. M.; Maze, J. R.; Le Sage, D.; Yeung, T. K.; Cappellaro, P.; Hemmer, P. R.; Yacoby, A.; Lukin, M. D.; Walsworth, R. L. Coherence of nitrogen-vacancy electronic spin ensembles in diamond. *Phys. Rev. B* **2010**, *82*, 201201.
- (24) Abtew, T. A.; Sun, Y. Y.; Shih, B.-C.; Dev, P.; Zhang, S. B.; Zhang, P. Dynamic Jahn-Teller Effect in the NV⁻ Center in Diamond. *Phys. Rev. Lett.* **2011**, *107*, 146403.
- (25) Maze, J. R.; Gali, A.; Togan, E.; Chu, Y.; Trifonov, A.; Kaxiras, E.; Lukin, M. D. Properties of nitrogen-vacancy centers in diamond: the group theoretic approach. *New J. Phys.* **2011**, *13*, 025025.
- (26) Grinolds, M. S.; Hong, S.; Maletinsky, P.; Luan, L.; Lukin, M. D.; Walsworth, R. L.; Yacoby, A. Nanoscale magnetic imaging of a single electron spin under ambient conditions. *Nat. Phys.* **2013**, *9*, 215–219.
- (27) Doherty, M. W.; Struzhkin, V. V.; Simpson, D. A.; McGuinness, L. P.; Meng, Y.; Stacey, A.; Karle, T. J.; Hemley, R. J.; Manson, N. B.; Hollenberg, L. C. L.; Prawer, S. Electronic Properties and Metrology Applications of the Diamond NV⁻ Center under Pressure. *Phys. Rev. Lett.* **2014**, *112*, 047601.
- (28) Bhandari, C.; Wysocki, A. L.; Economou, S. E.; Dev, P.; Park, K. Multiconfigurational study of the negatively charged nitrogenvacancy center in diamond. *Phys. Rev. B* **2021**, *103*, 014115.
- (29) Auburger, P.; Gali, A. Towards ab initio identification of paramagnetic substitutional carbon defects in hexagonal boron nitride acting as quantum bits. *Phys. Rev. B* **2021**, *104*, 075410.
- (30) Li, S.; Pershin, A.; Thiering, G.; Udvarhelyi, P.; Gali, A. Ultraviolet Quantum Emitters in Hexagonal Boron Nitride from Carbon Clusters. *J. Phys. Chem. Lett.* **2022**, *13*, 3150–3157.
- (31) Tawfik, S. A.; Ali, S.; Fronzi, M.; Kianinia, M.; Tran, T. T.; Stampfl, C.; Aharonovich, I.; Toth, M.; Ford, M. J. First-principles investigation of quantum emission from hBN defects. *Nanoscale* **2017**, 9, 13575.
- (32) Mendelson, N.; Chugh, D.; Reimers, J. R.; Cheng, T. S.; Gottscholl, A.; Long, H.; Mellor, C. J.; Zettl, A.; Dyakonov, V.; Beton, P. H.; Novikov, S. V.; Jagadish, C.; Tan, H. H.; Ford, M. J.; Toth, M.; Bradac, C.; Aharonovich, I. Identifying carbon as the source of visible single-photon emission from hexagonal boron nitride. *Nat. Mater.* **2021**, *20*, 321–328.
- (33) Klaiss, R.; Ziegler, J.; Miller, D.; Zappitelli, K.; Watanabe, K.; Taniguchi, T.; Alemán, B. Uncovering the morphological effects of high-energy Ga+ focused ion beam milling on hBN single-photon emitter fabrication. *J. Chem. Phys.* **2022**, *157*, 074703.
- (34) Dev, P. Fingerprinting quantum emitters in hexagonal boron nitride using strain. *Phys. Rev. Research* **2020**, *2*, 022050.
- (35) Dev, P.; Reinecke, T. L. Substrate effects: Disappearance of adsorbate-induced magnetism in graphene. *Phys. Rev. B* **2014**, *89*, 035404.
- (36) Manchanda, P.; Kumar, P.; Dev, P. Thickness dependence of hydrogen-induced phase transition in MoTe₂. *Phys. Rev. B* **2020**, *101*, 144104.
- (37) Naumov, I. I.; Dev, P. Quantum materials interfaces: Graphene/bismuth (111) heterostructures. *Phys. Rev. Research* **2020**, 2, 023157.
- (38) Manchanda, P.; Kumar, P.; Dev, P. Defect-induced 4p-magnetism in layered platinum diselenide. *Phys. Rev. B* **2021**, *103*, 144403.
- (39) Giannozzi, P.; Baroni, S.; Bonini, N.; Calandra, M.; Car, R.; Cavazzoni, C.; Ceresoli, D.; Chiarotti, G. L.; Cococcioni, M.; Dabo, I.; Dal Corso, A.; de Gironcoli, S.; Fabris, S.; Fratesi, G.; Gebauer, R.; Gerstmann, U.; Gougoussis, C.; Kokalj, A.; Lazzeri, M.; Martin-Samos, L.; Marzari, N.; Mauri, F.; Mazzarello, R.; Paolini, S.; Pasquarello, A.; Paulatto, L.; Sbraccia, C.; Scandolo, S.; Sclauzero, G.; Seitsonen, A.; Smogunov, A.; Umari, P.; Wentzcovitch, R. M.; Giannozzi, P.; et al. QUANTUM ESPRESSO: a modular and opensource software project for quantum simulations of materials. *J. Phys.: Condens. Matter* 2009, 21, 395502.
- (40) Wehling, T. O.; Lichtenstein, A. I.; Katsnelson, M. I. First-principles studies of water adsorption on graphene: The role of the substrate. *Appl. Phys. Lett.* **2008**, *93*, 202110.

- (41) Bermudez, V. M.; Robinson, J. T. Effects of Molecular Adsorption on the Electronic Structure of Single-Layer Graphene. *Langmuir* **2011**, 27, 11026–11036.
- (42) Dev, P.; Xue, Y.; Zhang, P. Defect-Induced Intrinsic Magnetism in Wide-Gap III Nitrides. *Phys. Rev. Lett.* **2008**, *100*, 117204.
- (43) Dev, P.; Zhang, P. Unconventional magnetism in semi-conductors: Role of localized acceptor states. *Phys. Rev. B* **2010**, *81*, 085207.
- (44) Dev, P.; Zeng, H.; Zhang, P. Defect-induced magnetism in nitride and oxide nanowires: Surface effects and quantum confinement. *Phys. Rev. B* **2010**, 82, 165319.
- (45) Noh, G.; Choi, D.; Kim, J.-H.; Im, D.-G.; Kim, Y.-H.; Seo, H.; Lee, J. Stark Tuning of Single-Photon Emitters in Hexagonal Boron Nitride. *Nano Lett.* **2018**, *18*, 4710–4715.
- (46) Lazić, S.; Espinha, A.; Pinilla Yanguas, S.; Gibaja, C.; Zamora, F.; Ares, P.; Chhowalla, M.; Paz, W. S.; Burgos, J. J. P.; Hernández-Mínguez, A.; Santos, P. V.; van der Meulen, H. P. Dynamically tuned non-classical light emission from atomic defects in hexagonal boron nitride. *Communications Physics* **2019**, *2*, 113.
- (47) Perdew, J. P.; Yue, W. Accurate and simple density functional for the electronic exchange energy: Generalized gradient approximation. *Phys. Rev. B* **1986**, *33*, 8800–8802.
- (48) Perdew, J. P.; Burke, K.; Ernzerhof, M. Generalized Gradient Approximation Made Simple. *Phys. Rev. Lett.* **1996**, 77, 3865–3868.
- (49) Wright, A. F.; Leadbetter, A. J. The structures of the β -cristobalite phases of SiO2 and AlPO4. Philosophical Magazine: A Journal of Theoretical Experimental and Applied Physics 1975, 31, 1391–1401.
- (50) Grimme, S. Semiempirical GGA-type density functional constructed with a long-range dispersion correction. *J. Comput. Chem.* **2006**, 27, 1787–1799.
- (51) Monkhorst, H. J.; Pack, J. D. Special points for Brillouin-zone integrations. *Phys. Rev. B* **1976**, *13*, 5188–5192.